International Journal of Multiphase Flow 36 (2010) 661–671

Contents lists available at ScienceDirect

International Journal of Multiphase Flow

journal homepage: www.elsevier.com/locate/ijmulflow

An appraisal of liquid–liquid slug flow in different pipe orientations

T.K. Mandal [a], G. Das [b,*], P.K. Das [c]

[a] Department of Chemical Engineering, National Institute of Technology, Durgapur 713 209, India
[b] Department of Chemical Engineering, Indian Institute of Technology, Kharagpur 723 302, India
[c] Department of Mechanical Engineering, Indian Institute of Technology, Kharagpur 723 302, India

ARTICLE INFO

Article history:
Received 11 December 2008
Received in revised form 25 March 2010
Accepted 11 April 2010
Available online 4 May 2010

Keywords:
Slug flow
Small diameter pipe
Undulated pipeline
Flow pattern

ABSTRACT

Gas–liquid slug flow occurs over a wide range of phase flow rates and in a variety of practical applications during gas–liquid two-phase flows. The range of slug flow increases further in narrow pipes (<0.0254 m), undulated pipelines, riser tube, etc. On the other hand, the past literature shows that slug flow is rarely observed for liquid–liquid cases. In the present study, an interest was felt to investigate whether liquid–liquid slug flow occurs in situations known for excessive slugging in gas–liquid cases. For this, experiments have been performed in narrow (0.012 m ID) vertical and horizontal pipes and an undulated pipeline of 0.0254 m internal diameter where the V-shaped undulation comprises of an uphill and a downhill section between two horizontal pipes. The studies have been performed for both peak and valley orientation of the undulation. Kerosene and water have been selected as the test fluids and the optical probe technique has been used to supplement visual observations especially at higher flow rates. The studies have revealed the existence of the slug flow pattern over a wide range of phase flow rates in all the three geometries. Interestingly, it has been noted that the introduction of an undulation induces flow patterns which bear a closer resemblance to gas–liquid flows as compared to liquid–liquid flows through a horizontal pipe of 0.0254 m diameter.

1. Introduction

Slug flow has a unique appearance distinctly different from the other flow patterns commonly observed during two-phase flow through horizontal and vertical pipes. This is primarily due to its intermittent character, which arises from the periodic appearance of large bullet-shaped bubbles termed as Taylor bubbles and liquid slugs occupying the space between two successive Taylor bubbles (Fig. 1a). The bubbles are usually axisymmetric and occupy the entire cross sectional area in a vertical tube. On the other hand, they are asymmetric and tend to slide along the upper pipe wall in a horizontal pipe. These have been designated as elongated gas plugs in Fig. 1b to distinguish them from Taylor bubbles observed in vertical tubes. Similar Taylor bubbles are observed in drinking straws when the glass is empty, the "riser" section of a coffee percolator and in the neck of a bottle, which is being emptied too rapidly.

The slug flow pattern is frequently encountered during two-phase flow. It is a common occurrence in various practical applications like geothermal, oil and gas wells, boiler tubes, thermosyphon reboilers, distillation column, absorption tower and heat exchangers, etc. The importance of this pattern has been further enhanced in the era of miniaturization since it occurs over a wider range of flow conditions in small diameter tubes. In addition, severe slugging has been reported in hilly terrains, undulated pipelines and riser tubes. As a result, a large number of studies, both experimental and theoretical, have been reported on gas–liquid slug flow in different geometries. Nevertheless, not much is known about liquid–liquid slug flow.

The past studies as shown in Tables 1 and 2 have reported that slug flow either does not occur or exists over a narrow range of flow conditions in different pipe orientations. This can be attributed to the inherent differences in the physics of gas–liquid and liquid–liquid flow situations. A survey of the past literature shows that only a few researchers have observed slug flow in narrow horizontal pipes. Beretta et al. (1997a,b) have identified the slug flow pattern and tried to predict the transition criteria and pressure drop of this flow pattern in a 0.003 m diameter horizontal pipe using existing models. They conducted the experiments using relatively high viscous oil as reported in Table 1. Recently, Wegmann and Rohr (2006) have also identified this flow pattern in 0.0056 m and 0.007 m diameter tubes during the simultaneous flow of paraffin and water. On the other hand, not much is known about slug flow in vertical pipes. The study by Hasan and Kabir (1999) has observed pseudo slug flow in plexiglass pipes of 0.0635 and 0.127 m diameter.

Considering the aforementioned facts, an interest was felt in the present work to see whether slug flow is observed during low viscosity oil–water flows in situations known for excessive slugging in gas–liquid systems. As mentioned earlier, these include flow in

* Corresponding author. Tel.: +91 3222 283952; fax: +91 3222 255303.
E-mail address: gargi@che.iitkgp.ernet.in (G. Das).

0301-9322/$ - see front matter © 2010 Elsevier Ltd. All rights reserved.
doi:10.1016/j.ijmultiphaseflow.2010.04.002

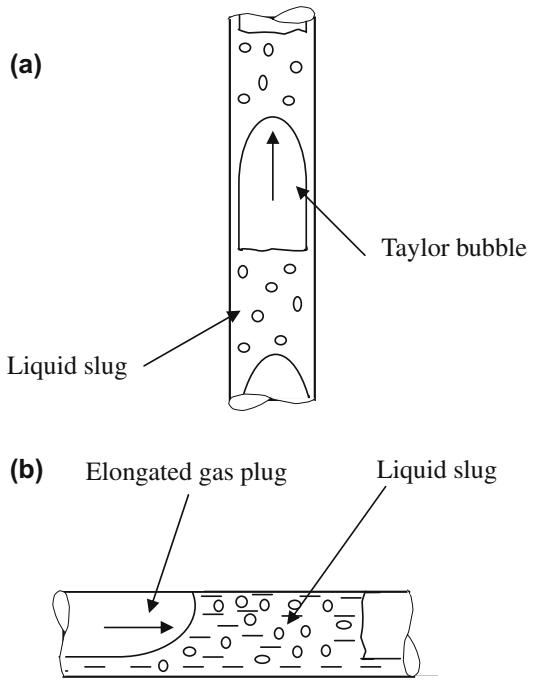

Fig. 1. A schematic of gas–liquid slug flow: (a) vertical pipe; (b) horizontal pipe.

small diameter pipes (<0.025 m) and undulated pipelines where the undulation comprises of an uphill or a downhill section between two horizontal portions. A detailed experimental study has been undertaken to observe slug flow and note its inception and termination to adjacent flow patterns with change of flow conditions. The study depicts the onset of slugging in an undulated pipeline. Further, a comparison with the corresponding flow conditions for kerosene–water flow through a 0.0254 m pipe diameter has revealed the influence of pipe diameter on the interfacial distribution. It may be noted that the two pipe diameters yield the value of Eotvos number ($Eo = \frac{(2\pi)^2\gamma}{\Delta\rho g D^2}$) as 0.94 and 3.4 respectively.

2. Experimental setup for investigation of slug flow

A schematic of the experimental setup is shown in Fig. 2. It consists of a fluid handling system (storage tanks, pumps and rotameters) and three different test rigs viz an undulated, a horizontal and a vertical section. These have been designated as TS1, TS2 and TS3 respectively in Fig. 2. TS2 and TS3 are acrylic pipes of 0.012 m diameter and 5 m length. Since the flow patterns have been compared with literature data in a 0.0254 m diameter pipe (Raj et al., 2005; Jana et al., 2006), care has been taken to use the same inlet geometries as used by the previous authors. Accordingly, the fluids are introduced by a T arrangement in TS3 and a special mixer described by Raj et al. (2005) in TS2. TS1 comprises of an uphill and a downhill section connecting two horizontal pipes. It is of uniform diameter of 0.0254 m throughout its length. The different dimensions and nomenclature of the undulated pipeline have been described in Fig. 3. Experiments have been performed for both peak and valley configurations. The peak comprises of an uphill and a downhill section in order in the direction of flow whereas the reverse arrangement makes up the valley configuration. The horizontal sections are referred to as upstream and downstream sections according to the direction of fluid flow. The junction of the upstream and uphill region is termed as the uphill elbow and that between the downhill and downstream section is the downhill elbow. The angle of inclination is 4° with respect to the horizontal for both uphill and downhill portions. All the test

Table 1
List of the literature for horizontal oil–water flow.

Authors	Pipe ID and material	μ_o/μ_w	ρ_o/ρ_w	σ, N/m	Observed flow patterns
Russell et al. (1959)	0.0203 m Cellulose Acetate-Butyrate	20.13	0.84	–	SM, $D_{O/W}$ B_o
Guzhov et al.(1973)	0.039 m steel	21.8	0.898	0.0448	SM, $D_{W/O}$, $D_{O/W\ \&\ W}$ $D_{W/O\ \&\ O/W}$
Valle and Kavandal (1995)	0.0375 m Glass	2.55	0.792	37.3	SM, $D_{O/W,\ \&\ W}$ $D_{W/O\ \&\ O/W}$
Beretta et al. (1997a,b)	0.003 m Glass	61.67	0.87	0.0315	D, B, intermittent, A Pressure drop
		45.49	0.877	0.036	
		8.55	0.874	0.0374	
Nadler and Mewes (1997)	0.059 m perspex	18–35	0.848	–	SM, $D_{O/W\ \&\ W}$, $D_{O/W}$, $D_{W/O}$, $D_{W/O\ \&\ O/W}$, $D_{W/O\ \&\ W}$
Angeli and Hewitt (2000)	0.0243 and 0.024 m acrylic	1.6	0.803	0.017	$D_{O/W}$, $D_{W/O}$, $D_{O/W\ \&\ W}$, $D_{W/O\ \&\ O}$, $D_{W/O\ \&\ O/W}$
Angeli et al. (2002)	0.038 m stainless steel	5.25	0.828	0.0447	SW, $D_{O/W}$, $D_{W/O\ \&\ O/W}$, $D_{W/O}$
Chakrabarti et al. (2005)	0.025 m PMMA	1.2	0.787	0.045	SS, SW, P, $D_{O/WW}$, TL, ID
Raj et al. (2005)	0.025 m PMMA	1.2	0.787	0.045	SS, SW, P, $D_{O/WW}$, TL, ID
Wegmann and Rohr (2006)	0.0056 and 0.007 m glass	6.14–5.78	0.820–0.822	0.0622	Stratified, annular, intermittent, dispersed

Table 2
List of the literature for vertical oil–water flow.

Authors	Pipe ID and material	μ_o/μ_w	ρ_o/ρ_w	σ, N/m	Work done
Govier et al. (1961)	0.0264 m cellulose acetate-butyrate	0.936	0.78	35.3	Holdup, pressure drop
		20.1	0.851	50.2	
		150	0.88	49.8	
Brown and Govier (1961)	0.0264 m cellulose acetate-butyrate	21.5	0.85	50.34	Pressure drop, bubble velocity, bubble size distribution
Flores et al. (1998)	0.051 m acrylic	20	0.858	35.5	Flow pattern (DO/W, VFD O/W, O/W CF), holdup and pressure drop
Zavareh et al. (1988)	0.184 m acrylic	2.46	0.783	–	Bubble flow
Hasan and Kabir (1999)	0.0635 and 0.127 m plexiglass	1.544	0.756		Flow pattern (bubbly flow, pseudoslug flow, and churn flow), drift velocity of the lighter oil phase
Hamad et al. (2000)	0.078 m perspex	1.6	0.803	17	Drop velocity, size distribution
Simmons and Azzopardi (2001)	0.063 m PVC	1.125	0.684	10	Drop size distribution
Jana et al. (2006)	0.025 m perspex	1.2	0.787	45	Flow pattern (B, DB, CT, CA) parallel wire conductivity probe

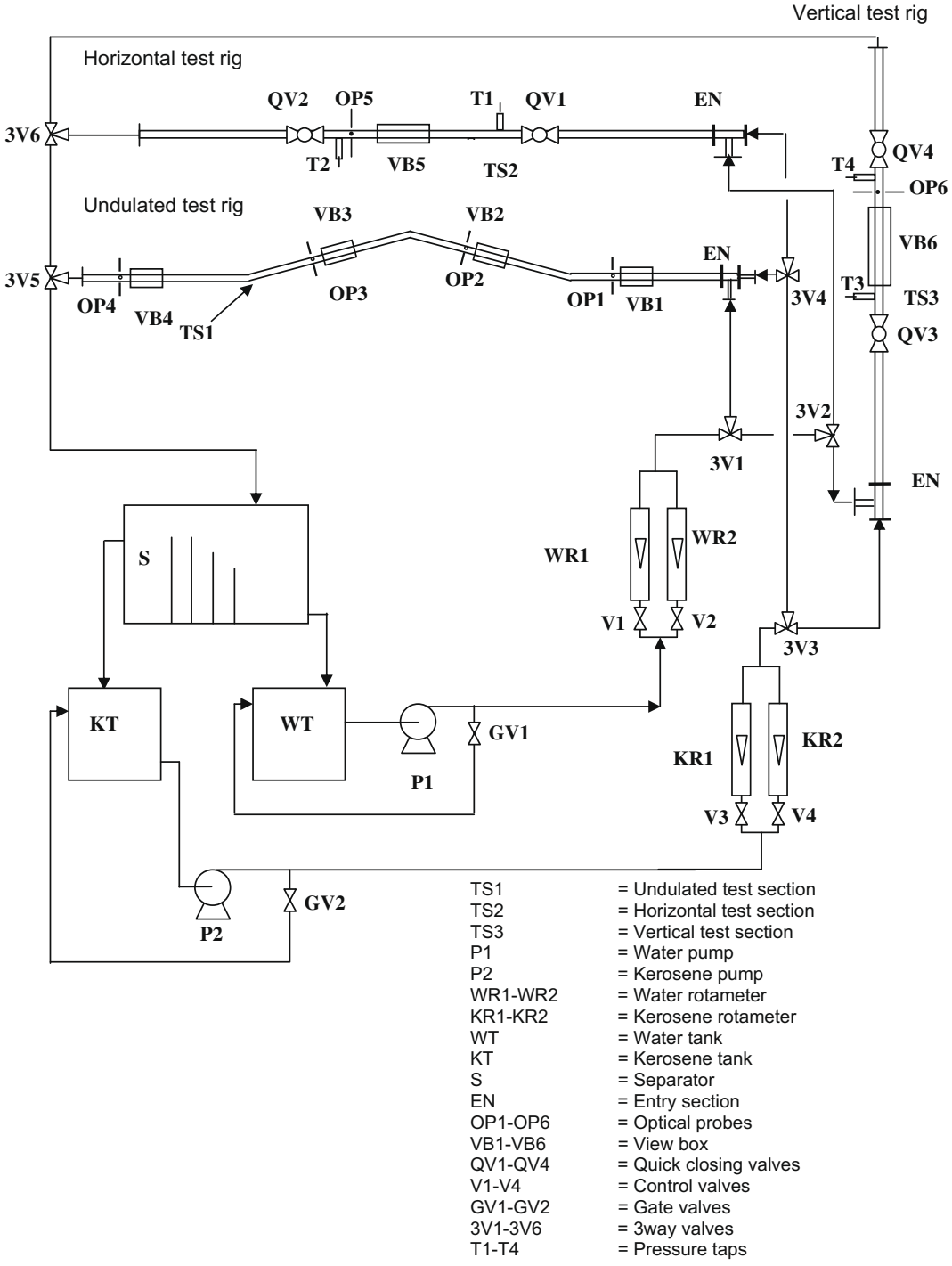

Fig. 2. A schematic of the experimental setup.

sections are made of perspex for visualization and photography of the interfacial distributions.

Dyed kerosene (density = 787 kg/m^3, viscosity = 1.2 mPa s at 20 °C and 101.33 kPa) and water (density = 1000 kg/m^3, viscosity = 1 mPa s at 20 °C and 101.33 kPa) are used as the test fluids. The value of contact angle for water–kerosene system with perspex has been measured as 68° using goniometer. All the properties have been measured several times during the entire period of experimentation and a maximum variation of ±1% have been noted. Oil and water are pumped to the entry section of the test rig through precalibrated rotameters. The specifications of the rotameters for both the fluids are 0–1.67 $\times$ 10^{-4} m^3/s with a least count of 1.67 $\times$ 10^{-6} m^3/s and 0–1.0 $\times$ 10^{-3} m^3/s with the least count of 1.67 $\times$ 10^{-5} m^3/s. The error in flow rate measurement using these two rotameters are ±4% and ±2% respectively. This has been supplied by the manufacturer and also verified by calibration under the present conditions.

The flow of the fluids is directed to the desired section by a set of six three-way valves (3V1–3V6) as shown in the figure. After flowing through the test rig, the two-phase mixture enters separator (S) where the phases are separated by gravity. The water and kerosene are recycled back to the respective storage tank. Experiments are performed over a wide range of fluid superficial velocity to study slug flow pattern and note its onset and termination from

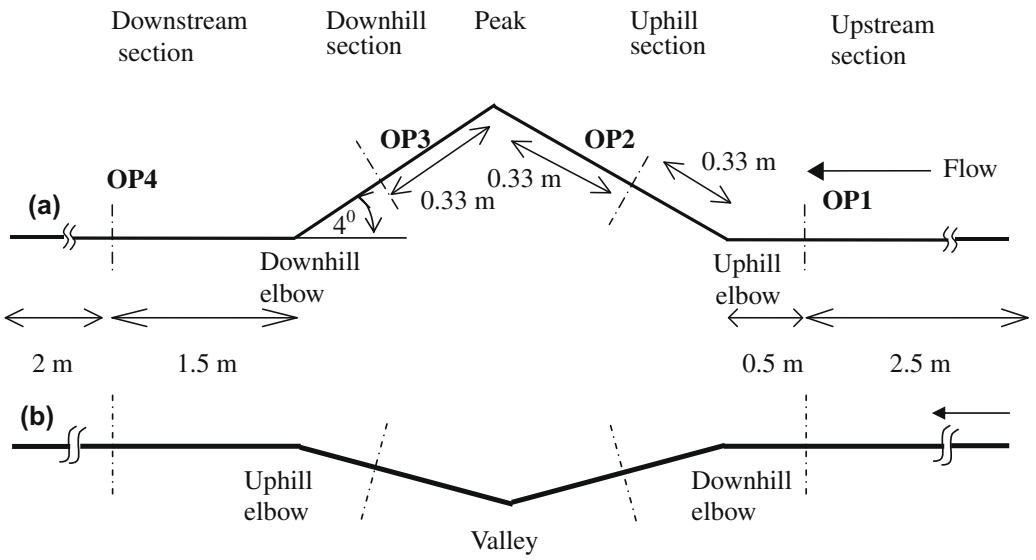

Fig. 3. Nomenclature and dimensions of the different sections of the undulated pipeline: (a) peak configuration; (b) valley configuration.

the adjacent distributions. The superficial velocity of water (U_{SW}) and kerosene (U_{SK}) are varied from 0.04 to 1.93 m/s and from 0.02 to 1.73 m/s respectively in the present experiments. The uncertainty in velocity measurement has been estimated as ±4% and ±2% for higher and lower flowrates respectively for both the pipes.

3. Identification of flow patterns

The interfacial distribution has been estimated from visual and photographic observations. The transparent acrylic pipes used for all the rigs have enabled this exercise. A digital camera (SONY DSC F717) is used for photography. View boxes (VB1–VB6) have been installed in the different sections of the undulated pipeline and small diameter pipes to minimize the image distortion during photography. They are rectangular boxes made of perspex and filled with glycerol which has a refractive index (1.47) close to perspex (1.49). Considerable care has been taken to ensure that the view boxes are placed centrally away from the entry and exit sections in order to eliminate end effects. View boxes VB1 and VB4 are placed at $L/D = 98$ and 231 respectively from the entry section, while VB2 and VB3 are placed at $L/D = 15$ from either elbows. VB5 and VB6 are placed at $L/D = 212$ from the entry section.

The visualization studies have been observed to be ineffective at high phase flow rates. So the non-intrusive optical probe technique as described by Jana et al. (2007) has also been adopted to identify the flow patterns particularly at high phase flow rates. Six optical probes (OP1–OP6 in Fig. 2) have been installed for this purpose. Probes OP1–OP4 are installed at different position of the undulated pipeline as shown in Fig. 3. Probe OP1 is located at the upstream section at a distance of 2.5 m ($L/D = 100$) from the entry region. OP2 and OP3 are placed at the midpoint of the uphill (or downhill in case of valley configuration) and downhill (or uphill in case of valley configuration) section of the test rig respectively. Probe OP4 is located at the downstream portion at a distance of 1.5 m ($L/D = 60$) from the downhill elbow (uphill elbow for valley configuration) and 2 m ($L/D = 80$) prior to the exit of the pipeline in order to eliminate end effects. Probes OP5 and OP6 are placed at a distance of 2.6 m ($L/D = 217$) from the entry section of the horizontal and vertical pipes respectively as shown in Fig. 2. Signals obtained from the sensors are used to supplement the visual and photographic technique wherever necessary (especially at higher phase velocities). The process diagram of the optical measurement is shown in Fig. 4. It comprises of a He–Ne laser source (~2 mW, ~632.8 nm wavelength and 2 mm beam diameter), a light dependent resistance (LDR) detector and a processing circuit data logger unit and a computer. The laser source serves as a source of monochromatic laser light. The LDR sensor is located at the diametrically opposite point to detect light transmitted by the laser source after its passage through the test section. The narrow laser beam passes through the two-phase medium before falling on the LDR and the intensity is converted into voltage by the processing circuit. The resultant voltage is sent to the computer through the data logger unit. The basic working principle of the optical probe and description of processing circuit are provided by Jana et al. (2007). The probe signals have been normalized ($V^* = \frac{V - V_{min}}{V_{max} - V_{min}}$) with respect to the voltages obtained during single-phase flow of either of the fluids. Since kerosene has a higher absorption coefficient, it yields the lower output voltage (V_{min}) while water gives the higher voltage (V_{max}). Different signal analysis techniques namely, Probability Density Function (PDF) analysis and fast Fourier transform (FFT) have been used for a better appraisal of the flow phenomena. The statistical moments of the PDF curves namely mean (m), var-

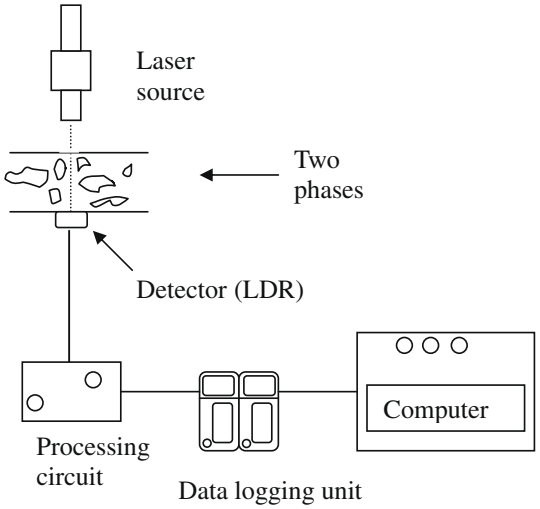

Fig. 4. Schematic representation of the optical diagnostics.

iance (σ) and skewness (S) are used for an objective identification of the flow patterns. The details of the analyses have been mentioned by Jana et al. (2007).

The reproducibility of the results was checked by recording the signals for longer time periods under different combinations of phase velocities in the different flow patterns. Different windows of time span 10 s have been selected from the same continuous signal and the PDFs have been constructed from them. The moments exhibit high repeatability and agree within ±4% for all the cases with a time span of 10 s or more. So a time period of 2 min is selected for recording the probe signals.

4. Result and discussion

The flow patterns as observed in test sections TS1, TS2 and TS3 are discussed in sequence. In the following discussion and relevant figures, U_{SK} and U_{SW} indicate the respective superficial velocities of kerosene and water. For the comparative study, the flow pattern maps has been represented with Froude number of the individual liquids as the co-ordinate axes where the respective Froude number for kerosene and water has been defined (Zapke and Kroger, 2000) in terms of their superficial velocity as,

$$\mathrm{Fr_K} = \frac{U_{SK}\sqrt{\rho_K}}{\sqrt{\Delta\rho g D}} \quad (1)$$

and

$$\mathrm{Fr_W} = \frac{U_{SW}\sqrt{\rho_W}}{\sqrt{\Delta\rho g D}} \quad (2)$$

In the equations, ρ_K and ρ_W are the densities of kerosene and water and $\Delta\rho = \rho_W - \rho_K$.

4.1. Flow patterns in 0.012 m diameter vertical pipe

The flow phenomena as obtained from the probe signals and their PDF and FFT analysis along with the photographic observation has been presented in Fig. 5. The normalized probe signals have been shown near the photograph while the PDF curve has been placed just above the probe signal. In the curves m, σ and S represent the mean, standard deviation and skewness respectively. The ratio of low to high voltage peak denoted as ROP is mentioned for the bi-modal PDFs of the slug flow pattern. The FFT curves are shown near the PDF curves (right top corner of each panel).

Fig. 5a reveals that at low kerosene velocity (U_{SK} = 0.13 m/s), oil plugs (They are smaller in size. They assume the nose shape of Taylor bubbles but do not have a well developed tail region. They are intermediate between the droplets characterizing bubbly flow and Taylor bubble characterizing slug flow) are distributed in the continuous water phase. The corresponding probe signal indicates a square like wave fluctuating between two steady values of the normalized voltage. The higher value corresponds to water phase and the lower value to kerosene phase as mentioned earlier. This hints at the alternate appearance of the two phases and is further evident from the bi-modal nature of the PDF curve where the smaller left hand peak indicates a smaller proportion of in situ kerosene in the flow passage. Discrete Taylor bubbles (It is bigger in size and has a distinct nose and a tail region as shown in Fig. 5b.) appear with increasing kerosene velocity (U_{SK} = 0.26 m/s) as is evident

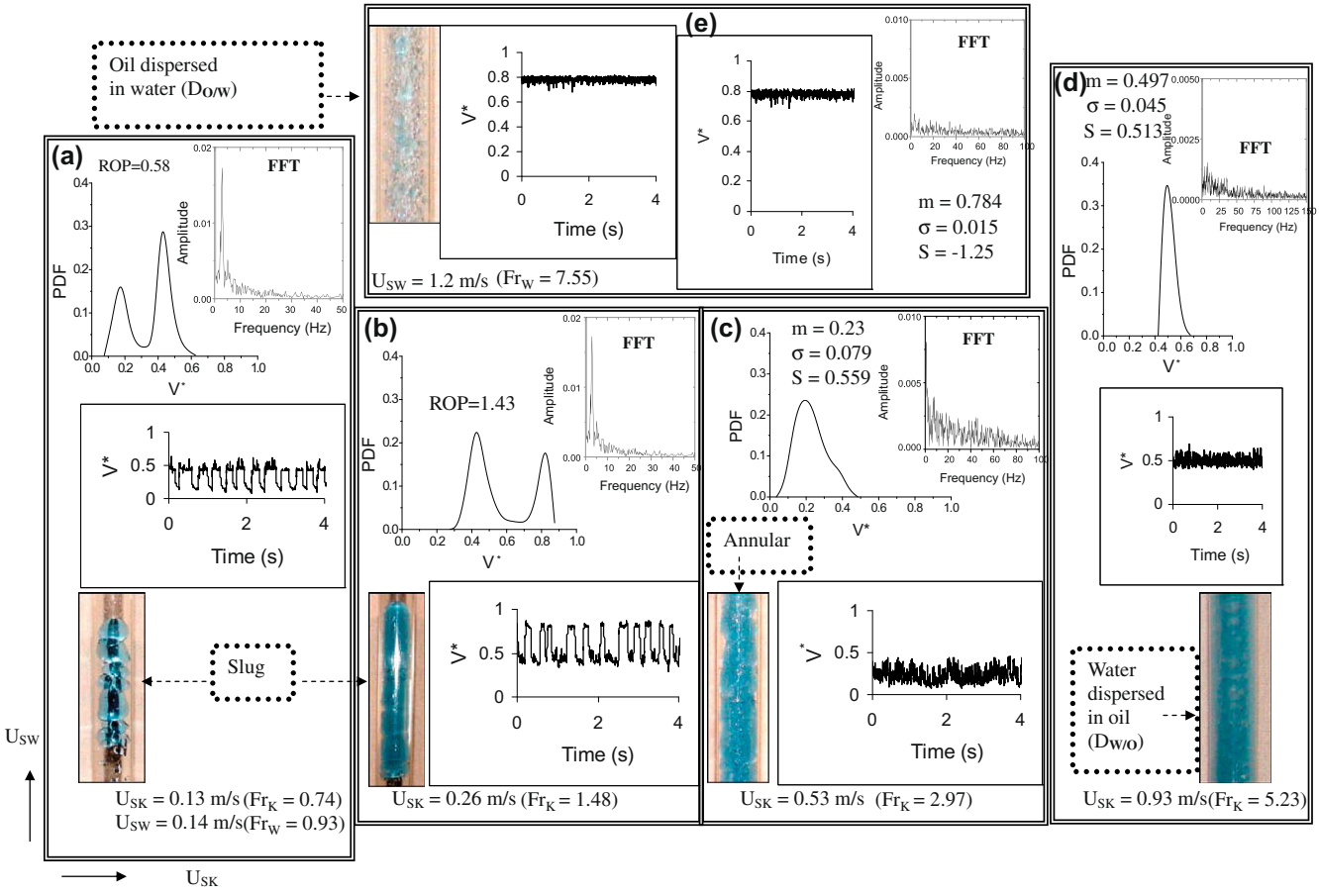

Fig. 5. Photograph, probe signals, their PDF and FFT analysis for different phase velocities in a 0.012 m diameter vertical pipe. (m, σ, S and ROP represent the mean, standard deviation, skewness and ratio of low to high voltage peak respectively; $\mathrm{Fr_K}$ and $\mathrm{Fr_W}$ are defined by Eqs. (1) and (2).)

from the similar square wave nature of the probe signal and the bimodal PDF curve in Fig. 5b. It may be noted that similar PDF curves have been noted by Jones and Zuber (1975) during gas–liquid slug flow. The higher ROP in the latter case indicates the increased oil proportion with increase of oil flow rate as expected. The corresponding FFT curves in Fig. 5a and b are characterized by a peak at non-zero frequency. Hubbard and Dukler (1966) have suggested that such FFT curves with a dominating non-zero frequency to indicate slug flow where with the peak indicating the frequency of passage of the oil Taylor bubbles.

With a further increase in kerosene velocity, the Taylor bubbles become larger with a corresponding decrease in the length of the water bridge. This continues till the Taylor bubbles coalesce to form a continuous kerosene core along the center of the pipe and water forms an annular film around the kerosene phase. This is termed as annular flow. The corresponding probe signal gives a low value of mean voltage while a single peaked right skewed PDF is obtained at low V^*. The shift of the curve towards low V^* indicates the predominance of kerosene phase in the flow passage. A peak is obtained at zero frequency in the FFT of Fig. 5c. Its amplitude decreases with increase in frequency thus hinting at a separated flow pattern (Hubbard and Dukler, 1966). It may be noted that annular distribution of the two phases is not clear from visual and photographic observation and is confirmed from the nature of the PDF and FFT curves.

With increase in kerosene velocity, the amplitude of the interfacial waves increase and at a certain higher flow rate, the Kelvin–Helmholtz instability is so pronounced that the water film breaks down into small water droplets which penetrate into the continuous kerosene medium. This causes dispersion of water in kerosene. However, it may be noted that such a distribution is not evident from visualization studies. The photograph taken at U_{SW} = 0.14 m/s and U_{SK} = 0.93 m/s (Fig. 5d) shows that the whole test passage appears blue and the distribution of the water phase is not very clear. The PDF curve is characterized by a higher mean value as compared to core annular flow and a single peak with positive skewness and lower spread. The FFT of the signal is similar to band-limited white noise (Fig. 5c). These observations suggest water dispersed in oil ($D_{W/O}$) rather than a separated flow of the two phases under the given conditions.

Oil dispersed in water flow ($D_{O/W}$) is observed at a higher water superficial velocity. The corresponding signal shows an almost steady output at high mean value (0.784) and a low standard deviation. The PDF appears to be the mirror image of the one obtained under water dispersed in oil flows ($D_{W/O}$). It is left skewed and shifts towards V^* close to unity while the FFT under these conditions is similar to the FFT obtained for water dispersed in oil flows ($D_{W/O}$).

4.1.1. The corresponding flow pattern map

The information thus obtained is depicted graphically in the form of a flow pattern map in Fig. 6. As mentioned earlier, the Froude number of both phases has been selected as the co-ordinate axes. The range of existence of the slug flow pattern is marked by dotted lines in the map. It is observed to extend from U_{SK} = 0.13–0.46 m/s and U_{SW} = 0.14–0.8 m/s. The annular flow pattern is observed at moderate phase velocities. Here the kerosene core forces the water to flow along the wall of the pipe. It is observed for U_{SK} = 0.46–0.62 m/s and U_{SW} = 0.14–0.34 m/s. At higher kerosene velocity (U_{SK} > 0.7 m/s), water droplets remain dispersed in the kerosene medium while the reverse occurs at higher water velocity (U_{SW} > 0.8 m/s). These flow patterns are termed as water dispersed in kerosene ($D_{W/O}$) and oil dispersed in water ($D_{O/W}$) flows respectively in Fig. 6.

4.1.2. Comparison with flow pattern map obtained in a larger pipe diameter

For the comparative study, the flow pattern map given by Jana et al. (2006) for a kerosene–water flow through a 0.0254 m diameter vertical pipe has been superimposed on the flow pattern map obtained in the present work in Fig. 6. The different curves represent the transition boundaries of Jana et al. (2006) while the symbols indicate the various flow regimes obtained in the present study. From this figure, it is clear that at lower phase flow rates, Jana et al. (2006) has observed a bubbly flow pattern characterized by discrete irregular kerosene droplets dispersed in the continuous water medium whereas the present work reports slug flow. This is in agreement to the observation of Hewitt (1982) for gas–liquid flows. Moreover, the slug flow pattern observed in the present work extends over the entire range of bubbly flow and a part of

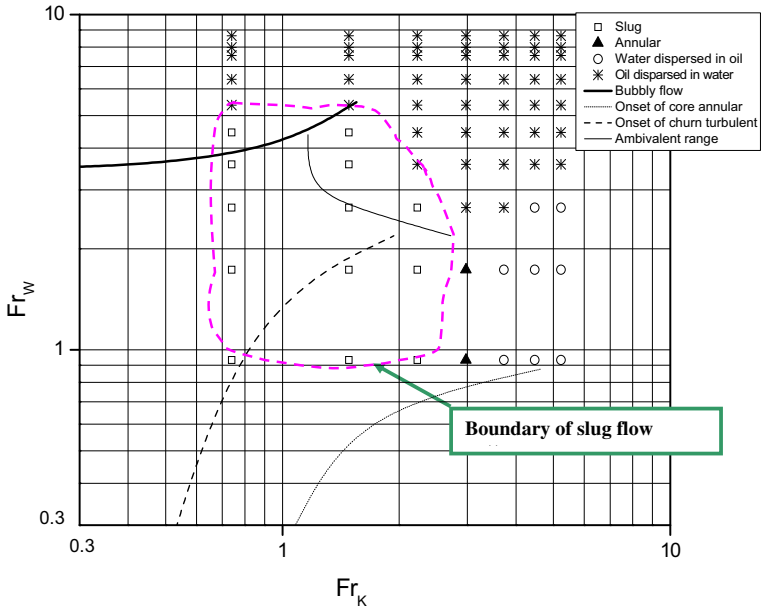

Fig. 6. Comparison of present flow pattern map for 0.012 m ID vertical pipe with the map reported by Jana et al. (2006) for a 0.0254 m diameter vertical pipe. (Symbols denote present work and curves indicate flow patterns as reported by Jana et al. (2006); Fr_K and Fr_W are defined by Eqs. (1) and (2) respectively.)

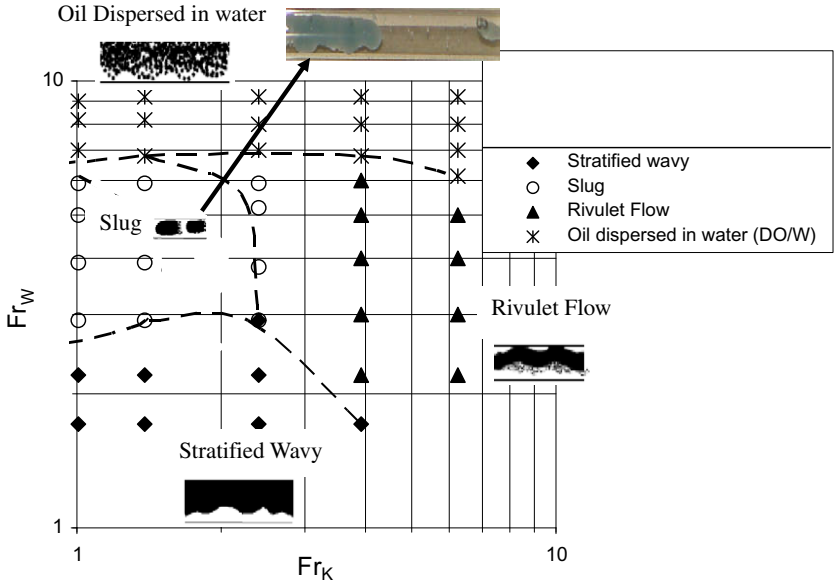

Fig. 7a. Flow pattern map for a 0.012 m diameter horizontal pipe (Fr_K and Fr_W are defined by Eqs. (1) and (2) respectively).

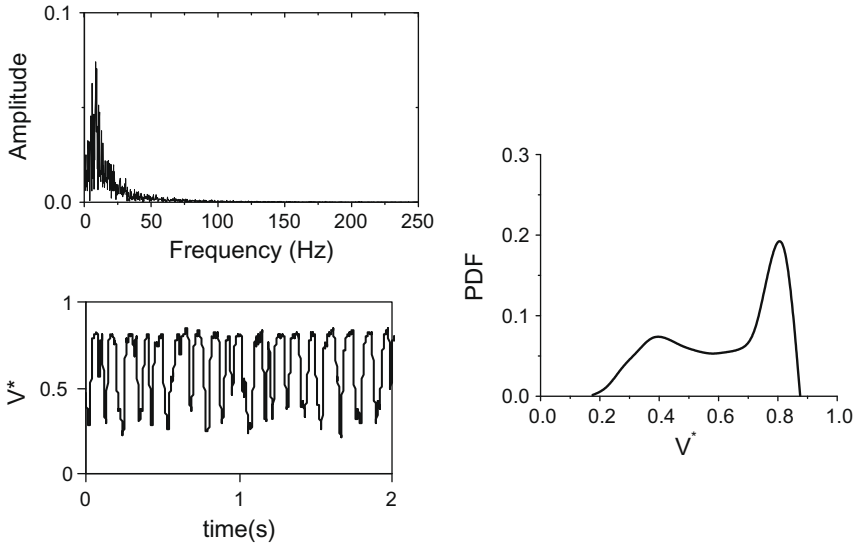

Fig. 7b. A typical probe signal and its characterization for slug flow pattern at U_{SW} = 0.8 m/s (Fr_W = 5.05) and U_{SK} = 0.35 m/s (Fr_K = 1.96).

churn-turbulent and core annular flow of the map reported by Jana et al. (2006). However, the transition from slug to dispersed flow is similar in both cases while the annular flow pattern in the 0.025 m ID pipe starts at lower phase flow rates and covers a wider range of the phase velocities as compared to that in the 0.012 m ID pipe. The churn-turbulent flow as reported by Jana et al. (2006) is similar to the churn flow of gas–liquid cases. No such pattern is obtained in the small diameter pipe. On the other hand, water dispersed in oil ($D_{W/O}$) flow pattern is observed in the present work but Jana et al. (2006) did not obtain this flow pattern within the range of parameters considered by them.

4.2. Flow patterns in a 0.012 m diameter horizontal pipe

Similar experiments have been performed in a horizontal pipe of 0.0127 m diameter. The flow patterns observed are represented in the form of a flow pattern map in Fig. 7a. The figure denotes the existence of the slug flow pattern over a wide range of flow conditions. The signal analysis of a typical slug flow pattern also presented in Fig. 7b at U_{SW} = 0.8 m/s and U_{SK} = 0.35 m/s.

In order to understand the influence of pipe diameter on the hydrodynamics of oil–water flow, the flow pattern map has been compared with the data provided by Raj et al. (2005) for kerosene–water flow through a 0.0254 m diameter horizontal pipe. The graphical comparison (Fig. 8) brings out a distinct influence of conduit dimension on interfacial configuration. In the larger pipe, the flow is smooth stratified at low phase flow rates and interfacial waviness sets in with increase in fluid velocities. The waviness breaks down to form a dense collection of drops between the oil layer at the top and water layer at the bottom. The three-layer pattern, as it is named, gives way to oil dispersed in water ($D_{O/W}$) flow at high water velocity and water dispersed in oil ($D_{W/O}$) at high oil flow. Fig. 8 indicates that smooth stratified flow is not observed in a small diameter pipe under the present set of experimental conditions. Slug flow covers a wide range of the flow pattern map in this geometry.

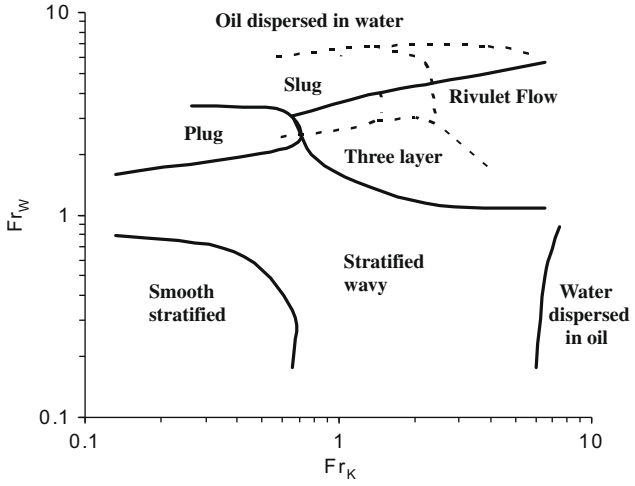

Fig. 8. A comparative study of the flow patterns as observed in horizontal 0.012 m ID and 0.0254 m ID pipe. (——— 0.0254 m ID pipe; - - - - 0.012 m ID pipe; Fr_K and Fr_W are defined by Eqs. (1) and (2) respectively).

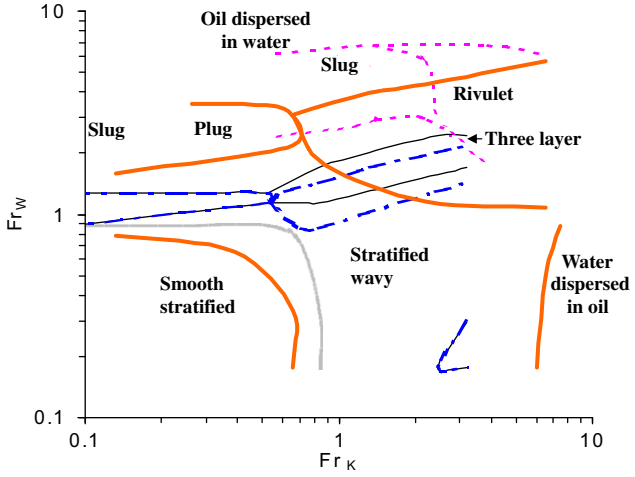

Fig. 9a. A comparative study of the flow patterns as observed in horizontal pipes under different conditions. (——— 0.0254 m ID horizontal pipe as reported by Raj et al. (2005); — — 0.012 m ID horizontal pipe of the present work; — downstream of a peak; – · – upstream of a peak; ▒▒▒▒▒▒ boundary of experimental data in undulated pipeline; Fr_K and Fr_W are defined by Eqs. (1) and (2).)

Moreover, the three-layer pattern, unique to liquid–liquid flows, does not appear in the present flow pattern map. It is therefore evident that the present map appears to bear a greater resemblance to gas–liquid flow than liquid–liquid flow in larger pipe diameters.

4.3. Flow regimes in the undulated pipe

The distinctive features of the flow regimes observed in the undulated pipe are described below and a comparative study has been reported between the flow regimes observed in the peak and the valley configuration.

4.3.1. Flow pattern map

The information obtained from the visual observations, photographs and optical probe analysis in the downstream and upstream sections of the peak orientation are presented as flow pattern maps in Fig. 9a. A sample analysis for characterization of slug is shown in Fig. 9b at U_{SW} = 0.23 m/s and U_{SK} = 0.02 m/s. The figure (Fig. 9a) reveals the existence of slug flow unlike the map reported by Raj et al. (2005). The bi-modal PDF curve and a peak at non-zero frequency in the FFT analysis of both figures (Fig. 9b1 and 9b2) confirm the visual observations. It may further be noted that smooth stratified flow has not been observed under the range of experimental conditions studied and the flow is stratified wavy at low velocities of the two liquids (U_{SK} = 0.05–0.73 m/s and U_{SW} = 0.04–0.36 m/s). Moreover, oil in water-dispersed ($D_{O/W}$) flow starts at a lower water velocity (U_{SW} = 0.33 m/s) and covers the entire range of kerosene superficial velocity from 0.02 to 0.73 m/s in the downstream section.

A comparison of the flow pattern maps obtained in the different sections reveals certain differences in the transition boundaries of the different sections. These boundaries are shown in Fig. 10. From the figure, it is clear that the transition boundaries of slug flow are almost the same for all the cases but there are differences in the transition from stratified wavy to three-layer and three-layer to dispersed flow. All the transition boundaries gradually shift towards higher values of superficial velocity from upstream to downstream section. Since the upper boundary of three-layer flow does not shift as much as the lower transition boundary, the area under three-layer flow decreases gradually as one moves along the pipeline in the direction of flow.

4.3.2. The phase distribution for valley configuration

The flow patterns in the valley configuration are similar to those observed in the peak configuration but there are slight differences in the range of existence of the different patterns particularly in the upstream section. Figs. 11 and 12 show the map for the upstream and downstream section respectively. In the figures the solid lines represent the boundaries of the peak configuration while the points denote the situation for the valley orientation.

Fig.11 shows that the inception of three-layer and dispersed flow occur at a lower water superficial velocity upstream of the valley as compared to the peak. Accordingly, the range of existence of stratified wavy flow becomes shorter in this case. A similar situation also arises for the slug flow regime. However, the transition boundary at the downstream section is not much affected by the presence of peak or valley. There are very small differences at the transition between stratified wavy to three-layer and three-layer to dispersed flow.

The differences arise because the downhill of valley configuration enhances the Kelvin–Helmholtz instability at the interface due to the effect of gravity. So the range of existence of stratified flow decreases and three-layer flow is initiated at lower velocities while the range of occurrence of dispersed flow increases. However this influence does not persist at the downstream section much away from the uphill elbow. So there is not much difference between the transition boundaries at downstream of the peak and valley.

4.3.3. Comparison with horizontal flow pattern map

Further attempts have been made to compare the aforementioned maps with the regimes reported for a horizontal pipe. For this, the downstream and upstream flow pattern maps of the peak orientation have been superimposed on the flow pattern map obtained by Raj et al. (2005) for horizontal pipes in Figs. 13 and 14 respectively. The fluid properties, pipe diameter and pipe material of Raj et al. (2005) and the present work are identical. The solid lines indicate the transitions as obtained by Raj et al. (2005) and the symbols represent data of the present work. The basic difference between the two is the existence of slug flow in the present case instead of the irregular plugs as reported in literature (Raj et al., 2005; Chakrabarti et al., 2005). Moreover, all the flow patterns start at a higher superficial velocity in the horizontal pipe

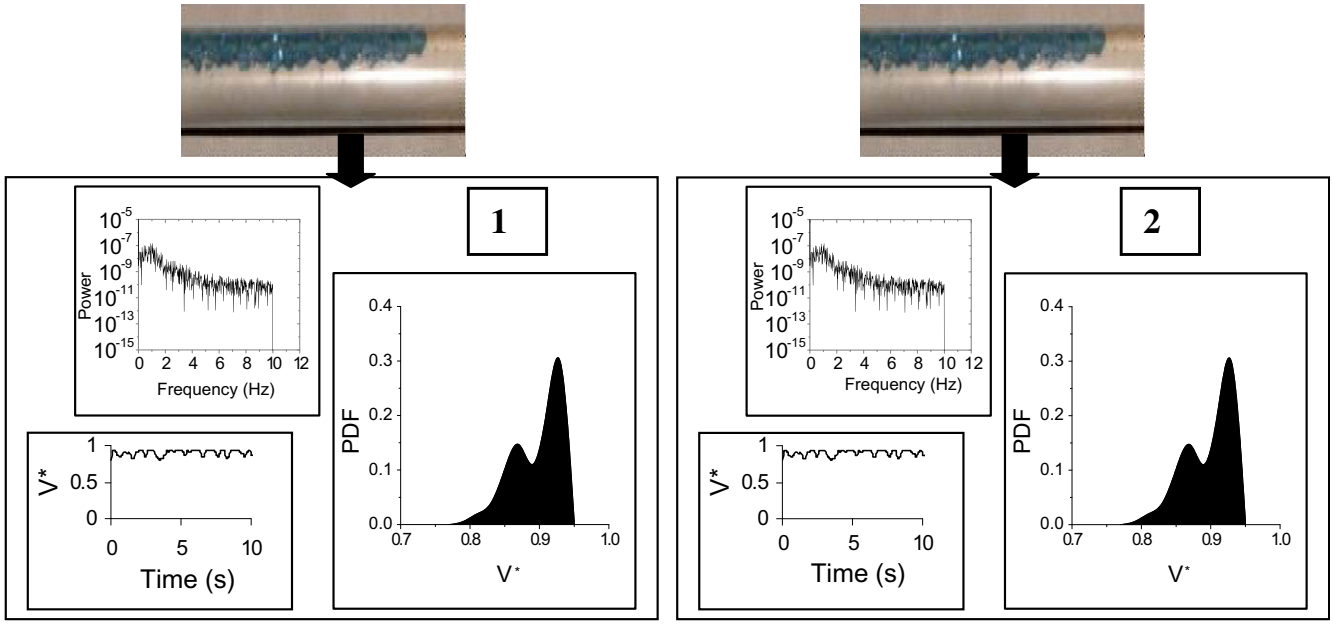

Fig. 9b. Characterisation of slug flow as observed in the upstream and downstream section of a peak orientation at U_{SW} = 0.23 m/s and U_{SK} = 0.02 m/s.

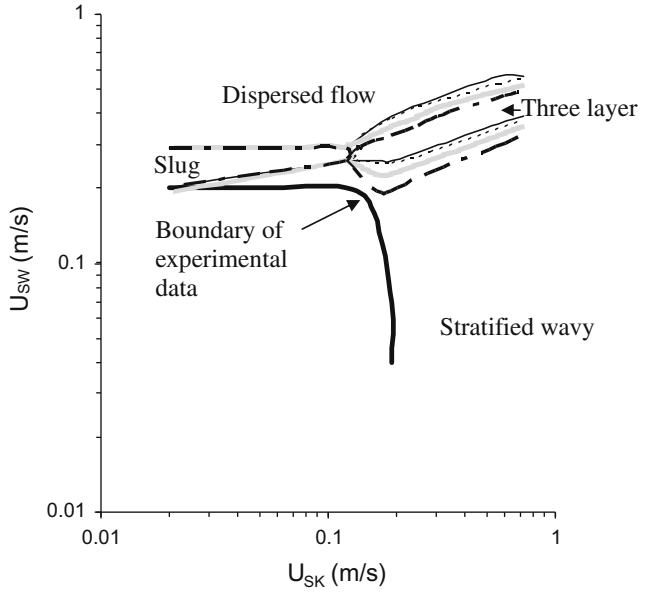

Fig. 10. Flow regime map of upstream, uphill, downhill and downstream sections in peak configuration. (— downstream flow pattern transition boundary; ——— boundary of experimental data; - - - - - downhill flow pattern transition boundary; uphill flow pattern transition boundary; – · – downstream flow pattern transition boundary.)

and the smooth stratified regime is totally absent in the undulated pipeline.

5. Reliability of the data processing

It may be noted that data processing is compared with visual observations for oil dispersed in water flow and slug flow under low phase velocities. They are then used to identify the patterns at high flow rates and pinpoint the transitions between flow patterns. For example, during slug flow the recorded signal contains alternate peaks and valleys and is characterized by a bi-modal PDF and a peak at non-zero frequency in the FFT curve. On the other hand, the oil dispersed in water flow is produced by a single peaked PDF at high voltage and a spread out FFT curve.

However, at high kerosene flows, it is difficult to distinguish between annular and water dispersed in oil flow. This is evident from the photograph of Fig. 5c and d. The entire passage appears to be blue and the distribution of water cannot be discerned distinctly. Under such conditions, the optical probe data is used to distinguish between them. For water dispersed in oil the PDF and FFT curves are mirror images of those obtained for oil dispersed in water flow while a FFT with a peak at zero frequency and a unimodal right skewed PDF at low V^* denotes core annular flow. Moreover, although slug flow can be distinguished from annular or oil dispersed in water flow visually, the transition is pinpointed by the disappearance of either of the peaks in the PDF curve.

6. Conclusions

In the present work, an interest was felt to note the influence of pipe diameter on liquid–liquid flow patterns. The pipe diameters for the comparative study have been selected as 0.012 m (Eo = 3.4) and 0.0254 m (Eo = 0.94). The experiments have showed marked differences in flow distribution for both horizontal and vertical orientation. Slug flow was found to exist over a wide range of flow conditions in the vertical as well as the horizontal narrow tube. A similar observation has been reported by Hewitt et al. (1986) for gas–liquid flows. This suggests that the information available for large tubes cannot be extended to predict the flow distribution in narrow tubes where surface forces dominate. Tubes of small diameters are particularly relevant in the present day scenario where compact reactor systems, heat exchangers and mass transfer equipment are preferred for higher yield at low investments.

Further studies have been performed to note the effects when a change in orientation occurs over short distances. This is inevitable in a practical plant layout, which has to accommodate several devices in a limited space. Such undulations also occur in hilly terrain pipelines during cross-country transportation. The experiments have revealed that undulations both in peak and valley configuration induce slugging in the upstream and downstream pipe. These

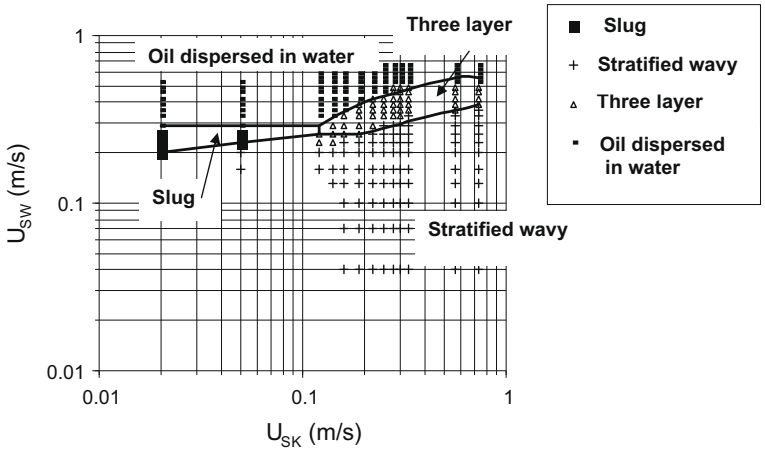

Fig. 11. Comparison of the upstream flow pattern maps as obtained for the valley and peak configuration. (Symbols denote flow patterns in valley configuration and solid lines indicate for flow pattern transitions in peak configuration.)

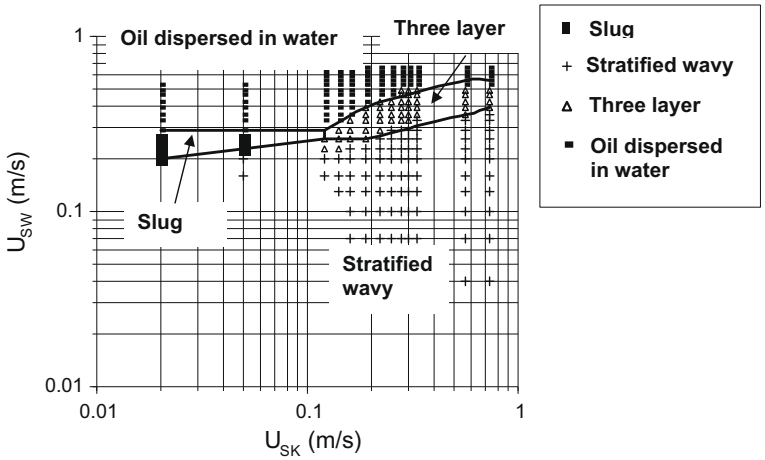

Fig. 12. Comparison of the downstream flow pattern maps as obtained for the valley and peak configuration. (Symbols denote flow patterns in valley configuration and solid lines indicate transition boundaries in peak configuration.)

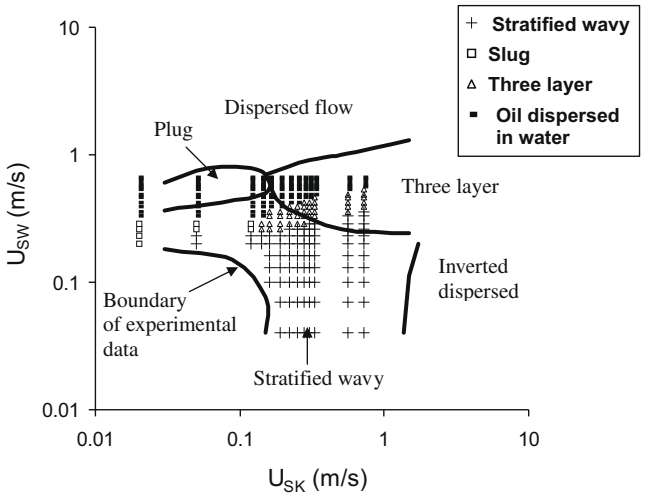

Fig. 13. A comparison of the downstream flow pattern map in peak configuration with the map obtained by Raj et al. (2005) in a 0.0254 m ID horizontal pipe. (Symbols denote present work and solid line represent transition boundary in Raj et al. (2005) map.)

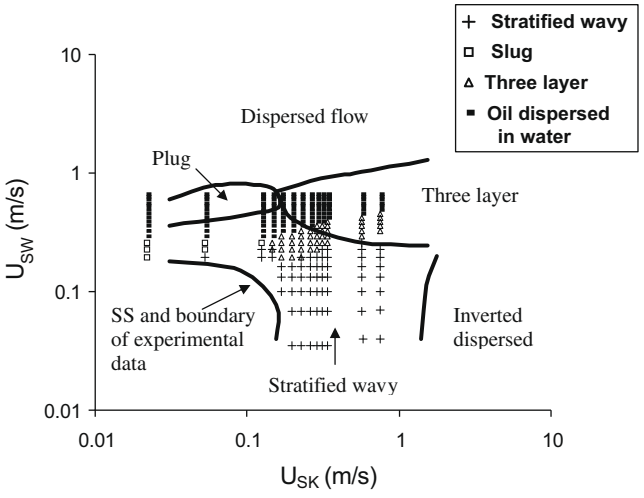

Fig. 14. A comparison of the upstream flow pattern map in peak configuration with the map obtained by Raj et al. (2005). (Symbols indicate present work and solid line denote Raj et al. (2005) map.)

facts need to be considered while predicting the flow patterns in long distance pipelines and practical applications.

References

Angeli, P., Hewitt, G.F., 2000. Flow structure in horizontal oil–water flow. Int. J. Multiphase Flow 26, 1117–1140.

Angeli, P., Lovick, S., Lum, Y.L., 2002. Investigations on the three-layer pattern during liquid–liquid flows. In: 40th European Two-Phase Flow Group Meeting, Stockholm, June 10–13.

Beretta, A., Ferrari, P., Galbiati, L., Andreini, P.A., 1997a. Horizontal oil–water flow in small diameter tubes: flow patterns. Int. Commun. Heat Mass Transfer 24, 223–229.

Beretta, A., Ferrari, P., Galbiati, L., Andreini, P.A., 1997b. Horizontal oil–water flow in small diameter tubes: pressure drop. Int. Commun. Heat Mass Transfer 24, 231–239.

Brown, R.A.S., Govier, G.W., 1961. High-speed photography in the study of two-phase flow. Can. J. Chem. Eng. 39, 159–164.

Chakrabarti, D.P., Das, G., Ray, S., 2005. Pressure drop in liquid–liquid two phase horizontal flow: experiments and prediction. Chem. Eng. Technol. 28, 1003–1009.

Flores, J.G., Sarica, C., Chen, T.X., Brill, J.P., 1998. Investigation of holdup and pressure drop behaviour for oil–water flow in vertical and deviated wells. Trans. ASME 120, 8–14.

Govier, G.W., Sullivan, G.A., Wood, R.K., 1961. The upward vertical flow of oil–water mixtures. Can. J. Chem. Eng. 9, 67–75.

Guzhov, A., Grishin, A.D., Medredev, V.F., Medredeva, O.P., 1973. Emulsion formation during the flow of two immiscible liquids. Neft. Choz. 8, 58–61 (in Russian).

Hamad, F.A., Pierscionek, B.K., Brunn, H.H., 2000. A dual optical probe for volume fraction, drop velocity and drop size measurements in liquid–liquid two-phase flow. Meas. Sci. Technol. 11, 1307–1318.

Hasan, A.R., Kabir, C.S., 1999. A simplified model for oil/water flow in vertical and deviated wellbores. SPE Prod. Facil. 141, 56–62.

Hewitt, G.F., 1982. In: Hetsroni, G. (Ed.), Hand Book of Multiphase System. Hemisphere Publishing Corporation, New York (Chapter 2).

Hewitt, G.F., Delhaye, J.M., Zuber, N., 1986. Multiphase Science and Technology, vol. 2. Hemisphere Publishing Corporation, Washington.

Hubbard, M.G., Dukler, A.E., 1966. The characterization of flow regimes for horizontal two-phase flow. In: Proc. Heat Transfer Fluid Mechanics Institute. Stanford University Press, pp. 100–121.

Jana, A.K., Das, G., Das, P.K., 2006. Flow regime identification of two-phase liquid–liquid upflow through vertical pipe. Chem. Eng. Sci. 61, 1500–1515.

Jana, A.K., Mandal, T.K., Chakrabarti, D.P., Das, G., Das, P.K., 2007. An optical probe for liquid–liquid two-phase flows. Meas. Sci. Technol. 18, 1563–1575.

Jones, O.C., Zuber, N., 1975. The interrelation between void fraction fluctuations and flow pattern in two phase flow. Int. J. Multiphase Flow 2, 273–306.

Nadler, M., Mewes, D., 1997. Flow induced emulsification in the flow of two immiscible liquids in horizontal pipes. Int. J. Multiphase Flow 23, 55–68.

Raj, T.S., Chakrabarti, D.P., Das, G., 2005. Liquid–liquid stratified flow through horizontal conduit. Chem. Eng. Technol. 28, 899–907.

Russell, T.W.F., Hodgson, G.W., Govier, G.W., 1959. Horizontal pipeline flow of mixtures of oil and water. Can. J. Chem. Eng. 37, 11–17.

Simmons, M.J.H., Azzopardi, B.J., 2001. Drop size distribution in dispersed liquid–liquid pipe flow. Int. J. Multiphase Flow 27, 843–859.

Valle, A., Kavandal, H.K., 1995, Pressure drop and dispersion characteristics of separated oil–water flow. In: Proceedings of the International Symposium on Two-Phase Flow Modelling and Experimentation, Italy, October 9–11.

Wegmann, A., von Rohr, P.R., 2006. Two phase liquid–liquid flows in pipes of small diameters. Int. J. Multiphase Flow 32, 1017–1028.

Zapke, A., Kroger, D.G., 2000. Countercurrent gas–liquid flow in inclined and vertical ducts – II. The validity of the Froude–Ohnesorge number correlation for flooding. Int. J. Multiphase Flow 26, 1457–1468.

Zavareh, F., Hill, A.D., Podio, A.L., 1988. Flow in vertical and inclined oil/water flow in pipes. Paper SPE 18215, Presented at the 63th Annular Technical Conference and Exhibition, Houston, TX, October 2–5.